

Applications of scintillators in optical-fiber-based detectors

Watanabe, Kenichi

Department of Applied Quantum Physics and Nuclear Engineering, Kyushu University

<https://hdl.handle.net/2324/7168662>

出版情報 : Japanese Journal of Applied Physics. 62 (1), pp.010507-1-010507-8, 2022-11-21. 応用物理学会

バージョン :

権利関係 : © 2022 The Japan Society of Applied Physics



Applications of scintillators in optical-fiber-based detectors

Kenichi Watanabe

Department of Applied Quantum Physics and Nuclear Engineering, Kyushu University, 744 Motooka,
Nishi-ku, Fukuoka 819-0395, Japan

*Email of corresponding author: k-watanabe@nucl.kyushu-u.ac.jp

Abstract

This article presents fundamentals and an overview of the optical-fiber-based scintillation detectors, which consist of a scintillator and an optical fiber light guide. This type of detector is preferentially used in special applications. In these applications, only a scintillator probe is placed in a severe environment, while a photodetector stays in a mild environment. Additionally, a detector should not disturb an irradiation field. As examples, applications in nuclear reactor physics experiments, medical uses, such as radiation therapies, and severe radiation conditions are reviewed.

KEYWORDS: *ionizing radiation; scintillator; optical fiber; nuclear reactor physics experiment; radiation therapy; radiation resistance*

1. Introduction

Scintillators have been used as ionizing radiation detectors in various applications, such as medical use¹⁾²⁾³⁾⁴⁾, radiation monitoring⁵⁾⁶⁾, security purpose⁷⁾⁸⁾⁹⁾, high energy physics¹⁰⁾¹¹⁾ and so on. Scintillation detectors basically consist of a scintillator and photodetector such as photomultiplier tube (PMT) or Si photodiode (PD). It is important to efficiently transport scintillation photons to a photodetector. Generally, there is difference in refractive indices between a scintillator and window material of the photodetector. The optical matching between a scintillator and photodetector window should be considered to efficiently transport scintillation photons to the photodetector. In some cases, a photodetector might be placed far from a scintillator. Generally, photodetectors have low resistance to a severe environmental condition compared with scintillators. Therefore, in applications, in which detectors should be used in severe conditions, only a scintillator probe is placed in a severe environment, while a photodetector stays in a mild environment. In this case, the scintillator and photodetector should be connected with a long light guide. In addition, in many applications, a detector should not disturb an irradiation field. Therefore, the detector size is desired to be small in these applications. Generally, a scintillator size can easily be small but a photodetector has a certain size. In this case, only the scintillator probe is placed at a measurement point, while the photodetector is placed at a point where the photodetector makes less influence on the irradiation field. As a light guide which can efficiently transport scintillation photons for a long distance, optical fibers are frequently applied. A number of optical-fiber-based scintillation detectors are developed and used in various applications.

In this paper, recently developed applications of scintillators in optical-fiber-based radiation detectors are reviewed. Scintillating fiber detectors are also optical-fiber-based detectors. The scintillating fiber is a scintillator and also works as a light guide. By using the scintillating fibers, a large size detector can easily be fabricated. Therefore, this type of detector is frequently used in high energy physics applications¹²⁾. Although, a number of detectors using scintillating fibers are developed, these detectors are outside the scope of this paper. This paper focuses on detectors using an optical fiber as a light guide to transport photons from a scintillator to a photodetector. First, the fundamentals of light collection and transportation using an optical fiber is described. And then, various applications of scintillators in optical-fiber-based detectors are reviewed.

2. Fundamentals of light collection and transportation using an optical fiber

When considering transport of photons from a scintillator to a photodetector, we should take the famous Snell's law into account. When a photon enters from region A to B, the Snell's law can be written as

$$n_A \sin \theta_A = n_B \sin \theta_B \quad (1),$$

where n_A and n_B are refractive indices of the region A and B, respectively. θ_A and θ_B are incident and refractive angles, which are photon direction angles from the normal vector of the interface between region A and B as shown in **Fig. 1 a)**. When we are considering photon transport in an optical fiber, the important phenomenon is the total internal reflection. Since the maximum angle of refraction is 90 degrees, the total internal reflection occurs when the incident angle is larger than the critical angle θ_c given by

$$\sin \theta_c = \frac{n_B}{n_A} \quad (2).$$

In this condition, the incident light is perfectly reflected without any loss as shown in **Fig. 1 b)**. An optical fiber is a light guide having less transmission loss using the total internal reflection. **Figure 2** shows the geometrical relation on pathways of scintillation photons in the optical fiber. As shown in **Fig. 2 a)**, photons in the transmission mode, in which photons with a larger reflection angle than the critical angle are reflected by the total internal reflection, can be transmitted with little loss. On the other hand, photons outside the transmission mode are refracted but escape out from the optical fiber. Since the critical angle is relatively large, acceptable angle into the transmission mode is usually small. The optical fiber light guide has low attenuation but small light collection efficiency. From this viewpoint, the important parameter of the optical fiber is the numerical aperture (NA). The NA is defined as

$$(NA) = n \sin \theta_{\max} = n_{\text{core}} \sin \left(\frac{\pi}{2} - \theta_c \right) = \sqrt{n_{\text{core}}^2 - n_{\text{clad}}^2} \quad (3),$$

where n is the refractive index of the medium around the fiber (in this case, the scintillator), θ_{\max} is the maximum acceptable angle into the fiber, n_{core} and n_{clad} are the refractive indices of the optical fiber core and cladding, θ_c is the critical angle. This parameter is an index of the acceptable angle into the optical fiber. As

shown in **Fig. 2 b)**, scintillation photons coming from outside the acceptable angle escape out from the optical fiber. Therefore, it is important to select high NA optical fiber for efficient light collection. On the other hand, when the optical fiber is used in an intense radiation field, the radiation damage of the fiber should be taken care, because the high NA fibers might have long path length in the optical fiber transmission mode. As you can see from **Eq. 3**, it is difficult to introduce the scintillation photons into the transmission mode for a scintillator having a high refractive index. Since some heavy scintillators, which are suitable for gamma-ray detection, have a relatively high refractive index, it is important to keep this issue in mind. In addition, as shown in **Fig. 2 c)**, it is important to note that photons entering from a side surface of an optical fiber cannot be introduced into the transmission mode.

In order to efficiently collect scintillation photons, it is desired to place the scintillator within the core area on the end surface of an optical fiber. This is because it is difficult to put scintillation photons into the transmission mode from the outside the core region even if the scintillator is surrounded by a reflector. This means that the desired scintillator size is smaller than that of the optical fiber core. **Figure 3** shows a fundamental configuration of the optical-fiber-based scintillation detector. When using large size scintillator crystal, a lens optics assembly should be considered to be applied to put scintillation photons into the transmission mode from a large volume scintillator. Of course, since the lens assembly has relatively large volume, it is not appropriate to use this kind of optics when it is not desired to interfere the measured field by the detector itself.

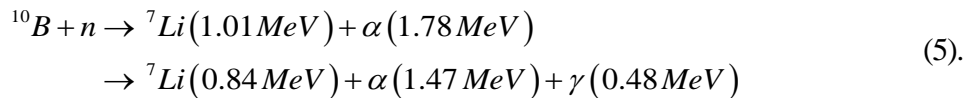
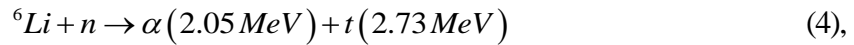
3. Applications of the fiber-based scintillator detectors

3.1 Nuclear reactor physics experiments

In nuclear reactor physics experiments, neutron detectors play an important role. Nuclear reactors are driven by nuclear fission chain reaction. A fission reaction is induced by neutron absorption and then releases two or three neutrons. In other words, the fission chain reaction is driven by neutrons. To measure the neutron intensity in a reactor, the reactor output can be determined. In addition, the neutron spatial distribution represents reactor power distribution. Therefore, the neutron detector is a fundamental tool in nuclear reactor

physics experiments. General neutron detectors used in the reactor physics experiments are fission chambers, ^3He proportional counters and BF_3 proportional counters. Since these types of the neutron detectors have a certain size, the detector insertion space should be secured in the moderator region of the experimental reactor. This insertion space makes an influence to the criticality of the reactor. The neutron activation method was conventionally applied to measure the neutron flux with small influence to the reactor criticality. In many cases, a gold foil or wire was used for the activation method. However, the activation method generally takes relatively long time for measurements. The activated sample is recovered after the shutdown of the reactor operation and then the induced gamma-rays from the sample are measured. Especially, when measuring the spatial distribution of the neutron flux, since a large number of the activated samples should be measured, the total measurement time becomes relatively long. In this kind of applications, online and small size neutron detectors are desirable.

One of the online and small size neutron detectors is an optical-fiber-based neutron detector, in which a small neutron scintillator containing nuclides with high neutron absorption cross-section, such as ^6Li and ^{10}B , is attached at the end of an optical fiber. The $^6\text{Li}(n, t)\alpha$ and $^{10}\text{B}(n, \alpha)^7\text{Li}$ reactions are important reactions for neutron detection and written as,



As describe above, these reactions emit highly energetic charged particles, which can directly excite a scintillator material. The optical-fiber-based neutron detector was first developed by Mori et al. and applied at the Kyoto University Critical Assembly (KUCA) for nuclear reactor physics experiments¹³⁾. The used detector in this application consisted of a plastic optical fiber with 0.8 mm core diameter and 2 m length, whose end was painted with a mixture of Ag:ZnS scintillator, LiF with 95% enriched ^6Li and adhesive paste in an weight ratio of 1:1:2 having a thickness of 0.3 mm, and a photomultiplier tube (PMT), which was connected to the other end of the fiber. Since this detector was quite small, it can be inserted into a narrow measuring hole in the critical assembly. The neutron scintillator, that is, a sensitive region of this detector can

1 be moved by a stepper-motor-based system. By moving the neutron scintillator position, the thermal neutron
2 flux distribution was measured. By using this detector, the spatial distribution of the neutron flux, which was
3 measured for 5 hours with a conventional gold wire activation method, was obtained in 10 min. Since the ${}^6\text{Li}$
4 neutron converter has higher cross-section for slower neutrons, this type of detector has a high sensitivity only
5 for thermal neutrons. This type of optical-fiber-based neutron detector were modified to improve some
6 detector characteristics¹⁴⁾¹⁵⁾. Although the plastic fiber has a high NA, the resistivity to radiation damage is
7 lower than a quartz fiber. Therefore, an optical fiber was changed to the quartz fiber to prevent radiation
8 damage. In addition, a mixture of Ag:ZnS scintillator and adhesive paste is also sensitive to gamma-rays and
9 fast neutrons. To enhance the signal-to-noise ratio for thermal neutron events, the ${}^{235}\text{U}$ neutron converter,
10 which absorbs thermal neutrons with a high cross-section and then makes a fission reaction, was applied. A
11 nuclear fission reaction releases 40 times higher energy than a ${}^6\text{Li}(\text{n}, \text{t})\alpha$ reaction. Since the signal pulse
12 height induced by a fission reaction is quite large compared with a ${}^6\text{Li}(\text{n}, \text{t})\alpha$, gamma-ray and recoil proton
13 reactions, the signal discrimination between thermal neutrons and others becomes easier and clearer. For fast
14 neutron detection, the ${}^{232}\text{Th}$ converter was also applied. The fission threshold energy of ${}^{232}\text{Th}$ is more than 1.1
15 MeV, so that the neutron detection probe using the ${}^{232}\text{Th}$ converter is sensitive only to fast neutrons. By
16 optical-fiber-based neutron detectors using the ${}^{235}\text{U}$ and ${}^{232}\text{Th}$ converters, the thermal and fast neutron
17 distributions were separately determined in the core of KUCA.

18 Although the ${}^{232}\text{Th}$ neutron converter is suitable for fast neutron detection, the use of ${}^{232}\text{Th}$ is limited to
19 the facilities authorized to use nuclear materials and requires the labor and time for controlling these materials.
20 In addition, since ${}^{232}\text{Th}$ is an alpha decay nuclide, the signal to noise ratio is low especially for weak neutron
21 fields because of background alpha events. Therefore, the optical-fiber-based detectors using alternative
22 converter materials for fast neutron detection were developed^{16),17)}. In these researches, some threshold
23 reactions of zinc and sulfur isotopes in Ag:ZnS scintillator, such as ${}^{64}\text{Zn}(\text{n}, \text{p}){}^{64}\text{Cu}$ and ${}^{32}\text{S}(\text{n}, \text{p}){}^{32}\text{P}$ reactions,
24 were proposed to be applied for fast neutron detections. This type of detector demonstrated to measure the
25 spatial distribution of fast neutrons emitted from an accelerator-based $\text{T}(\text{d}, \text{n})$ reaction neutron generator,
26 which was used for the accelerator driven system (ADS) experiments. In these experiments, the pulse shape

discrimination (PSD) technique was shown to be useful for eliminating noise signals induced in a PMT and optical fiber by Cherenkov events and so on.

The optical-fiber-based detectors using neutron converters and Ag:ZnS scintillator were quite useful for reactor physics experiments. However, a weak point of this type of detector was quite low sensitivity. Since a mixture of neutron converter, Ag:ZnS scintillator and adhesive paste is clouded, an amount of the neutron converter adhered on an end surface of an optical fiber is limited up to 0.3 mm thick at most. In order to increase an amount of the neutron converter, a wavelength-shifting fiber (WLSF) was applied. As described in chapter 2, photons entering from a side surface into an optical fiber cannot be introduced into the transmission mode. This is because the neutron converter materials should be adhered on an end surface of the optical fiber. **Figure 4** shows the schematic drawing of the WLSF. Although an optical fiber cannot accept photons into the transmission mode from a side surface in general cases, an incident photon from a side surface of the WLSF will be absorbed in the core and then a wavelength-shifted photon will be re-emitted. These re-emitted and wavelength-shifted photons can be transmitted in the transmission mode with little loss. The WLSFs are generally designed to pass through the wavelength-shifted photons in the core. The core material of the WLSF has strong absorption for incident scintillation photons and small attenuation for wavelength-shifted photons. Consequently, the WLSF can collect and transmit photons incident from the side surface. Yagi et al. developed the optical-fiber-based neutron detector using the WLSF and neutron scintillator for nuclear reactor physics experiments¹⁸⁾¹⁹⁾. Especially for sub-criticality determination experiments, in which the neutron flux in the core was not so high, the detector sensitivity was desired to be increased. The WLSF (Kuraray, Y11) with a 1 mm diameter and 10 mm long was connected with a plastic optical fiber with the same diameter, which was just used to transmit wavelength-shifted photons to a photodetector. The absorption peak wavelength of this WLSF is 430 nm, which roughly matches with the emission wavelength of LiF (450 nm), and its emission wavelength is 476 nm. A mixture of ⁶LiF converter, Ag:LiF scintillator and adhesive paste was coated onto the outer surface of the WLSF. Another end of the plastic fiber was connected with the PMT. Since the area of the WLSF side surface is much larger than the end surface area of the optical fiber, the effective amount of the neutron converter or the neutron detection sensitivity is much improved. The

neutron sensitivity was experimentally evaluated to be 10 times higher than the conventional one. The sensitivity was further improved by extending the neutron converter and WLSF region. When using a 200-mm long WLSF, since it was equivalent to take moving average with 200-mm, the resolution of the spatial distribution measurements was deteriorated. The sensitivity was enhanced by 10 times compared with one using a 10-mm long WLSF. This type of detector successfully demonstrated to measure the prompt neutron decay constant, which is a related parameter to the subcriticality of the reactor¹⁹⁾.

Since a mixture of the neutron converter, Ag:ZnS scintillator and adhesive paste was clouded, the converter thickness was limited up to 0.3 mm at most. In order to increase the converter thickness, the use of a transparent neutron scintillator is desirable. For a real-time subcriticality monitoring system, a highly sensitive optical-fiber-based neutron detector was developed using the WLSF and a large number of small pieces of a transparent neutron scintillator²⁰⁾. As a transparent neutron scintillator, LiF/Eu:CaF₂ eutectic scintillator was applied, which shows intense scintillation and has a high content of a ⁶Li converter²¹⁾. A huge number of small LiF/Eu:CaF₂ scintillator pieces with about 200-μm size was adhered on the side surface of the WLSF with a 100-mm long. The WLSF was connected to an end of a quartz optical fiber with a 10-m long. Since the scintillator containing a ⁶Li neutron converter is transparent and each scintillator piece has sufficient size to stop energetic charged particles generated in ⁶Li(n, t)α reaction, all neutron events show almost the same signal pulse height. Consequently, the fabricated detector showed a clear peak in the signal pulse height spectrum. This feature brings an advantage of the sensitivity stability against signal gain changes to this detector. Using high-speed signal processing module, the fabricated detector successfully demonstrated to determine the sub-criticality in real-time in the reactor physics experiments.

3.2 Medical uses

Ionizing radiation is widely used in medical applications. In these applications, it is important to assess the dose irradiated to patients and/or medical workers. For the dose assessment or dosimetry, optical-fiber-based scintillator detectors can be applied. Medical applications using ionizing radiation are categorized into two fields: radiological diagnosis and radiation therapy. In the radiological diagnosis, X-ray

1 with an energy less than 150 keV is mainly used. On the other hand, various types of ionizing radiation are
2 applied in radiation therapies. The used scintillators or detector configurations are selected depending on the
3 types of the measured radiation fields: the types of ionizing radiation, intensity and so on. In most cases, the
4 organic plastic scintillators are applied because they have similar mass and electron densities as those of water
5 and human tissue. Therefore, they have interaction properties with photons and/or electrons similar to water
6 and human tissue, that is, water-equivalent property²²⁾²³⁾. However, the organic plastic scintillators generally
7 show a lower light yield than inorganic scintillators. When irradiating an optical fiber with ionizing radiation,
8 the optical fiber itself slightly emit photons. This might be caused by a weak scintillation or Cherenkov
9 radiation processes in the optical fiber. This is frequently called as the stem effect²⁴⁾. In the case when the high
10 signal-to-noise ratio is low because of the stem effect, the brighter inorganic scintillators are selected.

11 In the diagnostic applications, the diagnostic X-ray has relatively low energy. These low energy X-ray
12 photons generate no Cherenkov radiation photon. Consequently, the stem effect is not severe in diagnostic
13 applications. This is because the plastic scintillators are selected in most diagnostic applications²⁵⁾²⁶⁾²⁷⁾²⁸⁾²⁹⁾³⁰⁾.
14 In addition, if the plastic optical fiber is used, all components of the detector is composed of only light
15 elements and makes little influence to the X-ray diagnosis²⁷⁾. The energy spectrum of the diagnostic X-ray
16 depends on the X-ray tube acceleration voltage. Therefore, the detector response on the tube voltage was
17 evaluated in detail²⁵⁾²⁶⁾²⁹⁾³⁰⁾. Since the reliability is quite important in medical applications, various
18 characteristics, such as temperature, optical-fiber bend radius and angular dependence, were evaluated²⁶⁾²⁸⁾.

19 In the radiation therapy applications, various types of ionizing radiations are applied, such as high energy
20 electrons, high energy X-rays, gamma-rays, protons, heavy ions, and neutrons. The dosimeter should be
21 designed depending on the radiation types. For radiation therapies, high energy photons, such as X-rays and
22 gamma-rays, are also applied. A significant difference from the diagnostic X-rays is their energy. The high
23 energy photons used in radiation therapies generate high energy electrons in an optical fiber. These high
24 energy electrons might have higher velocity than the threshold one for the emission of Cherenkov radiation.
25 This induces the stem effect, which causes an undesired dosimeter output generated in an optical fiber light
26 guide²⁴⁾. There are major three ways to compensate the influence of the Cherenkov radiation. The first one is

1 to use the dual optical fiber configuration, in which two optical fibers are located in the same
 2 arrangement⁽²²⁾⁽²³⁾⁽³¹⁾. An optical fiber is connected to the scintillator, but another one is just located in the same
 3 arrangement. Since the stem effect occurs in the both optical fibers, the effect can be compensated by taking
 4 the difference between the both. The second one is to use an bright inorganic scintillator, such as Tb:Gd₂O₂S
 5 (Tb:GOS) and Tl:CsI⁽³²⁾⁽³³⁾⁽³⁴⁾⁽³⁵⁾⁽³⁶⁾⁽³⁷⁾. Since the stem effect, such as the Cherenkov radiation, is generally small,
 6 it can be negligible by using bright scintillators. The final one is to apply the spectral difference between the
 7 scintillation and Cherenkov radiation⁽³⁸⁾⁽³⁹⁾. Since the Cherenkov radiation shows blue dominant and
 8 broad-spectrum emission, the probe signal can be extracted from the emission spectrum by using a scintillator
 9 showing longer wavelength and/or narrow spectrum emission. For radiation therapy applications, since the
 10 tissue-equivalent property is important, the plastic scintillator is ideal from this viewpoint. Some of this type
 11 of dosimeter are commercially available⁽⁴⁰⁾⁽⁴¹⁾. However, since the plastic scintillators show a not so high light
 12 yield, the dual optical fiber configuration is preferably applied to compensate the stem effect⁽²²⁾⁽²³⁾⁽³¹⁾. In some
 13 cases, the plastic scintillator showing green emission, such as BCF-60, is applied to use the spectral separation
 14 of the stem effect⁽³⁸⁾. Although the dosimeter system becomes a little bit complicated to compensate the stem
 15 effect, the plastic scintillator-based system shows various ideal features, such as tissue equivalence, energy
 16 independence, reproducibility, dose linearity, resistance to radiation damage, and near temperature
 17 independence. The inorganic scintillators can also be a promising candidate for radiation therapy applications.
 18 There are a number of bright inorganic scintillators, which can overcome the stem effect. Especially,
 19 scintillators showing green or longer wavelength emission have an additional advantage from a viewpoint of
 20 the spectral separation of the Cherenkov radiation. One of the promising inorganic scintillator materials is
 21 Tb:GOS, which shows a quite high light yield and green emission⁽³²⁾⁽³³⁾⁽³⁴⁾. Other inorganic scintillators are
 22 also considered to be applied for the radiation therapy applications. In order to improve the scintillation light
 23 collection efficiency, an inorganic scintillator is inserted inside the plastic fiber core⁽³²⁾⁽³⁷⁾. Since only the probe
 24 signal is enhanced in this method, the stem effect can relatively be reduced. Although inorganic scintillators
 25 show excellent scintillation features, it should be noted that they always suffer from an energy dependence of
 26 their responses, which causes a non-tissue-equivalent response⁽³⁷⁾.

For particle therapy applications, such as a proton therapy and carbon-ion therapy, the optical-fiber-based dosimeters have been considered to be applied. In these applications, an important task is to determine the maximum range of highly energetic charged particles, such as protons and carbon ions. Some organic and inorganic scintillators have been considered to be applied to the particle therapy applications⁴²⁾⁴³⁾⁴⁴⁾. In these applications, it is important to consider the quenching effect, which is caused by high linear energy transfer (LET) particles. According to the Birks model⁴⁵⁾, the scintillation light yield L per unit path length is written as,

$$\frac{dL}{dx} = \frac{S \frac{dE}{dx}}{1 + kB \frac{dE}{dx}} \quad (6),$$

where dE/dx : the stopping power or LET of an incident charged particle, S : the normal scintillation efficiency, and kB : the quenching factor. The quenching loss is large for high LET particle. Although the maximum range of incident charged particles can be determined, the quenching effect should be considered to evaluate an accurate dose for the both of organic and inorganic scintillators.

Boron neutron capture therapy (BNCT) is also one of the particle radiation therapies, but non-charged particle therapy. In BNCT, neutron capture agents containing boron are administrated into blood vessel of patients and carried preferentially into tumor cells. Then, thermal or epi-thermal neutrons are irradiated into the patient and $^{10}\text{B}(n, \alpha)$ reactions are induced. Reaction products, which are alpha particles and lithium nuclei, produce many ionizations in tumor cells and the tumor cells are damaged. The ranges of reaction products in tissues are comparable to the size of typical tumor cells. The damage is, therefore, limited into the cells accumulating boron neutron capture agents. It is, of course, important to evaluate the neutron intensity on a patient body surface. Therefore, an on-line and small optical-fiber-based neutron flux monitors have been developed.

The scintillators used in the optical-fiber-based neutron detectors for BNCT are categorized into two groups. One is a combined type of the neutron converter and scintillator. Another one is a scintillator containing the neutron converter. There are two candidate reactions used for neutron conversion to highly

energetic charged particles in neutron scintillators: ${}^6\text{Li}(n, t)\alpha$ and ${}^{10}\text{B}(n, \alpha){}^7\text{Li}$ reactions. As described above, high LET particles cause a severe quenching effect. From this viewpoint, the ${}^6\text{Li}$ converter has an advantage compared with ${}^{10}\text{B}$. In BNCT applications, the neutron detector should be insensitive to gamma-rays, which might induce undesired noise counts. The ${}^6\text{Li}$ converter also has an advantage even from a viewpoint of the neutron and gamma-ray discrimination owing to its highly energetic reaction products. Therefore, there was a detector using the ${}^{10}\text{B}$ converter in the early stages of development⁴⁶⁾, almost all detectors used the ${}^6\text{Li}$ converter. In the combined type neutron scintillators, the plastic scintillators and Ag:ZnS scintillator were applied. Since the former ones have fast response, they showed excellent counting rate capability and wide dynamic range⁴⁷⁾⁴⁸⁾⁴⁹⁾. However, since the plastic scintillator also responds to gamma-rays, the dual probe configuration, in which one uses a neutron converter but another uses only a scintillator, was applied to compensate the gamma-ray response. In the Ag:ZnS scintillator case, since the scintillator region was too thin to deposit an energy by a low LET electron generated in a gamma-ray interaction, the gamma-ray sensitivity was quite low⁵⁰⁾. However, since the converter layer was also limited, the neutron sensitivity was not sufficient. By applying the WLSF readout, the sensitivity of this type of detector was improved.

As a scintillator containing the ${}^6\text{Li}$ neutron converter, the detector using a Li glass scintillator was first developed⁵¹⁾. Since the Li glass scintillator also responds to gamma-rays, the dual probe configuration was applied again. The ${}^6\text{Li}$ and ${}^7\text{Li}$ enriched Li glass scintillators were combined. Since the ${}^7\text{Li}$ enriched scintillator has the same response to gamma-rays as the ${}^6\text{Li}$ enriched one but no neutron sensitivity, it can be used to compensate the gamma-ray response. As the next generation neutron scintillator, a quite bright Eu:LiCaAlF₆ scintillator was applied. To suppress the gamma-ray sensitivity in the single probe configuration, a new idea, in which the scintillator size was controlled to a few hundred micrometers, was proposed⁵²⁾.

Figure 5 shows the concept of gamma-ray suppression by controlling the scintillator size. In this scintillator, ${}^6\text{Li}(n, t)\alpha$ reaction products, alpha and triton, have quite short range of a few ten μm . On the other hand, fast electrons with about 1 MeV energy produced by gamma-ray interactions have relatively long range of the order of mm. If the scintillator size is controlled into a few hundred μm , the ${}^6\text{Li}(n, t)\alpha$ reaction products can deposit their whole energy but fast electrons escape to outside the scintillator with a large fraction of their

1 initial energy. Consequently, fast electrons induced by gamma rays can produce only signals with quite small
2 pulse height. Therefore, the neutron and gamma-ray discrimination was easily conducted in the pulse height
3 spectrum. In addition, since the Eu:LiCaAlF_6 scintillator is bright and transparent, the fabricated
4 optical-fiber-based detector showed a clear neutron peak in the pulse height spectrum shown in **Fig. 6**. This
5 feature is quite useful to easily set the discrimination level and assess the detector sensitivity and its stability.
6 The neutron sensitivity of this type of detector was quite low because a scintillation size was small. However,
7 it was not significant disadvantage because the neutron intensity in the BNCT irradiation field is quite high. A
8 low sensitivity in the BNCT applications might be a benefit to avoid the counting loss. The neutron sensitivity
9 of this type of detector was experimentally confirmed to be controlled by adjusting a scintillator size or mass
10 owing to its feature showing a neutron peak⁵³⁾. The neutron and gamma-ray discrimination ability was
11 slightly improved by utilizing the LiF/Eu:CaF_2 eutectics scintillator, which has higher Li content than
12 Eu:LiCaAlF_6 scintillator⁵³⁾. A high Li content helps to make a scintillator size small keeping the neutron
13 sensitivity. These type of neutron detectors were applied to evaluate the neutron intensity at the Nagoya
14 University Accelerator-based Neutron Source (NUANS), which was developed for the BNCT neutron
15 source⁵⁴⁾⁵⁵⁾. The measured results successfully agreed with the Monte Carlo simulation studies. From these
16 studies, it was concluded that the wall effect and the self-absorption effect should be taken into account to
17 accurately evaluate the neutron field by using a small ^6Li -enriched scintillator. Since the Eu:LiCaAlF_6 and
18 LiF/Eu:CaF_2 scintillators have microsecond order decay time, the counting rate capability is not excellent. By
19 changing the scintillator material to a fast Li glass scintillator, which has a few ten ns decay time, the counting
20 rate capability or dynamic range can be improved⁵⁶⁾. Various performances of this type of detector, such as
21 the thermal neutron sensitivity, output linearity, and gamma-ray response, were experimentally confirmed⁵⁷⁾.

23 3.3 Applications in severe radiation fields

24 The optical-fiber-based scintillation detectors are suitable for applications requiring high
25 radiation-resistance. One of the possible target applications is the radiation measurement at a high dose area in
26 a nuclear power plant. The radiation dose surveillance for the decommissioning of the Fukushima Dai-ichi

nuclear power station (1F) might be one of the target applications. In a severe radiation fields, the radiation damage of each component should be considered. Key components of the optical-fiber-based scintillation detector are a scintillator and optical fiber materials. Radiation damage or radiation resistance should be considered to design the detector system. Especially, since the optical fiber light guide has a long distance, a slight absorption induced by irradiating ionizing radiation can be a significant problem. There are various researches on development of the radiation-resistant optical fibers⁵⁸⁾⁵⁹⁾⁶⁰⁾. In addition, various radiation-resistant optical-fiber-based scintillation detectors were designed based on these knowledges⁶¹⁾⁶²⁾. These researches concluded that the silica optical fibers have a higher radiation resistance than the plastic ones and the radiation induced transmission loss is significant especially at the shorter wavelength region than 600 nm, which arises from creation of an E' center, non-bridging oxygen center and so on. In intense radiation fields, the stem effect caused by the Cherenkov radiation becomes severe especially in the blue spectral region. Based on these reasons, the longer wavelength or red region emission scintillators are considered to be suitable for the optical-fiber-based scintillation detectors used in a severe radiation circumstance⁶¹⁾⁶³⁾. The radiation-resistant optical-fiber-based dosimeter system using a Nd:Y₃Al₃O₁₂ (Nd:YAG) scintillator were developed and demonstrated in the Fukushima Dai-ichi Nuclear Power Station.

4. Conclusion

In the present review, the author introduced various applications using the optical-fiber-based scintillation detectors in addition to its fundamentals. Applications in nuclear reactor physics experiments, medical use, and severe circumstance, were focused. The detector configuration should be designed depending on requirements of each application. In addition, optical coupling between a scintillator and optical fiber is quite important for efficient light collection. For relatively new BNCT applications, some performance improvements were explained. A research on the radiation dose surveillance in the Fukushima Dai-ichi Nuclear Power Station was also introduced. Continuous studies will be required to develop compact and easy-to-use optical-fiber-based scintillation detectors. It is expected to extend the base of scintillator applications.

Acknowledgements

This work was supported in part by a program of "Development of Systems and Technology for Advanced Measurement and analysis" promoted by Japan Science and Technology Agency (JST) and a grant from the Association for Nuclear Technology in Medicine.

References

- 1) H. O. Anger, Nature **170**, 200 (1952).
- 2) C. L. Melcher, J. Nucl. Med. **41** [6], 1051 (2000).
- 3) S. Duclos, Interface-Electrochemical Soc. **7** [2], 34 (1998).
- 4) J. Krimmer, J. L. Ley, C. Abellan, J. P. Cachemiche, L. Caponetto, X. Chen, M. Dahoumane, D. Dauvergne, N. Freud, B. Joly, D. Lambert, L. Lestand, J. M. Létang, M. Magne, H. Mathez, V. Maxim, G. Montarou, C. Morel, M. Pinto, C. Ray, V. Reithinger, E. Testa and Y. Zoccarato, Nucl. Instruments Methods Phys. Res. Sect. A Accel. Spectrometers, Detect. Assoc. Equip. **787**, 98 (2015).
- 5) K. Watanabe, T. Yanagida, K. Fukuda, A. Koike, T. Aoki and A. Uritani, Sensors Mater. **27** [3], 269 (2015).
- 6) M. Lowdon, P. G. Martin, M. W. J. Hubbard, M. P. Taggart, D. T. Connor, Y. Verbelen, P. J. Sellin and T. B. Scott, Sensors **19** [18], 3828 (2019).
- 7) J. Glodo, Y. Wang, R. Shawgo, C. Brecher, R. H. Hawrami, J. Tower and K. S. Shah, Phys. Procedia **90** [November 2016], 285 (2017).
- 8) M. E. Ellis, K. Duroe and P. A. Kendall, Int. J. Mod. Phys. Conf. Ser. **44** [2010], 1660214 (2016).
- 9) K. Watanabe, T. Yamazaki, D. Sugimoto, A. Yamazaki, A. Uritani, T. Iguchi, K. Fukuda, S. Ishidu, T. Yanagida and Y. Fujimoto, Nucl. Instruments Methods Phys. Res. Sect. A Accel. Spectrometers, Detect. Assoc. Equip. **784**, 260 (2015).

- 1 10) P. Lecoq and M. Korzhik, IEEE Trans. Nucl. Sci. **47** [4], 1311 (2000).
- 2 11) T. Itoh, T. Yanagida, M. Kokubun, M. Sato, R. Miyawaki, K. Makishima, T. Takashima, T. Tanaka,
3 K. Nakazawa, T. Takahashi, N. Shimura and H. Ishibashi, Nucl. Instruments Methods Phys. Res. Sect.
4 A Accel. Spectrometers, Detect. Assoc. Equip. **579** [1], 239 (2007).
- 5 12) R. C. Ruchti, Annu. Rev. Nucl. Part. Sci. **46** [1], 281 (1996).
- 6 13) C. Mori, T. Osada, K. Yanagida, T. Aoyama, A. Uritani, H. Miyahara, Y. Yamane, K. Kobayashi, C.
7 Chihara and S. Shiroya, J. Nucl. Sci. Technol. **31** [3], 248 (1994).
- 8 14) C. Mori, A. Uritani, H. Miyahara, T. Iguchi, S. Shiroya, K. Kobayashi, E. Takada, R. F. Fleming, Y.
9 K. Dewaraja, D. Stuenkel and G. F. Knoll, Nucl. Instruments Methods Phys. Res. Sect. A Accel.
10 Spectrometers, Detect. Assoc. Equip. **422** [1–3], 129 (1999).
- 11 15) Y. Yamane, A. Uritani, T. Misawa, J. K. H. Karlsson and I. Pázsit, Nucl. Instruments Methods Phys.
12 Res. Sect. A Accel. Spectrometers, Detect. Assoc. Equip. **432** [2–3], 403 (1999).
- 13 16) T. Yagi, H. Unesaki, T. Misawa, C. H. Pyeon, S. Shiroya, T. Matsumoto and H. Harano, Appl. Radiat.
14 Isot. **69** [2], 539 (2011).
- 15 17) T. Yagi, K. Kondo, T. Misawa, K. Ochiai, S. Ohnishi, K. Takakura, S. Sato, C. Konno, C. H. Pyeon
16 and S. Shiroya, J. Nucl. Sci. Technol. **48** [5], 777 (2011).
- 17 18) T. Yagi, T. Misawa, C. H. Pyeon and S. Shiroya, Appl. Radiat. Isot. **69** [1], 176 (2011).
- 18 19) T. Yagi, C. H. Pyeon and T. Misawa, Appl. Radiat. Isot. **72**, 11 (2013).
- 19 20) K. Watanabe, M. Yamanaka, T. Endo and C. H. Pyeon, J. Nucl. Sci. Technol. **57** [2], 136 (2020).
- 20 21) N. Kawano, N. Kawaguchi, K. Fukuda, G. Okada and T. Yanagida, J. Mater. Sci. Mater. Electron. **29**
21 [11], 8964 (2018).
- 22 22) A. S. Beddar, T. R. Mackie and F. H. Attix, Phys. Med. Biol. **37** [10], 1883 (1992).
- 23 23) A. S. Beddar, T. R. Mackie and F. H. Attix, Phys. Med. Biol. **37** [10], 1901 (1992).
- 24 24) F. Theriault-Proulx, L. Beaulieu, L. Archambault and S. Beddar, Phys. Med. Biol. **58** [7], 2073
25 (2013).
- 26 25) F. Lessard, L. Archambault, M. Plamondon, P. Després, F. Theriault-Proulx, S. Beddar and L.

- 1 Beaulieu, Med. Phys. **39** [9], 5308 (2012).
- 2 26) D. E. Hyer, R. F. Fisher and D. E. Hintenlang, Med. Phys. **36** [5], 1711 (2009).
- 3 27) W. J. Yoo, D. Jeon, J. K. Seo, S. H. Shin, K. T. Han, W. S. Youn, S. Cho and B. Lee, Radiat. Meas.
- 4 **48** [1], 29 (2013).
- 5 28) S. Buranurak, C. E. Andersen, A. R. Beierholm and L. R. Lindvold, Radiat. Meas. **56**, 307 (2013).
- 6 29) J. Boivin, S. Beddar, C. Bonde, D. Schmidt, W. Culberson, M. Guillemette and L. Beaulieu, Phys.
- 7 Med. Biol. **61** [15], 5569 (2016).
- 8 30) M. R. Hoerner, E. J. Stepusin, D. E. Hyer and D. E. Hintenlang, Med. Phys. **42** [3], 1268 (2015).
- 9 31) A. S. Beddar, Radiat. Meas. **41** [SUPPL. 1], 124 (2006).
- 10 32) S. O’Keeffe, W. Zhao, W. Sun, D. Zhang, Z. Qin, Z. Chen, Y. Ma and E. Lewis, IEEE J. Sel. Top.
- 11 Quantum Electron. **22** [3], 35 (2016).
- 12 33) S. O’Keeffe, D. McCarthy, P. Woulfe, M. W. D. Grattan, A. R. Hounsell, D. Sporea, L. Mihai, I.
- 13 Vata, G. Leen and E. Lewis, Br. J. Radiol. [DOI:10.1259/bjr.20140702].
- 14 34) M. Alharbi, S. Gillespie, P. Woulfe, P. McCavana, S. O’Keeffe and M. Foley, IEEE Sens. J. **19** [6],
- 15 2140 (2019).
- 16 35) L. Ding, Q. Wu, Q. Wang, Y. Li, R. M. Perks and L. Zhao, EJNMMI Phys.
- 17 [DOI:10.1186/s40658-020-00327-6].
- 18 36) Y. H. Kim, M. W. Seo and J. W. Park, J. Nucl. Sci. Technol. **45**, 542 (2008).
- 19 37) Y. Hu, Z. Qin, Y. Ma, W. Zhao, W. Sun, D. Zhang, Z. Chen, B. Wang, H. Tian and E. Lewis,
- 20 Sensors Actuators, A Phys. **269**, 188 (2018).
- 21 38) J. M. Fontbonne, G. Iltis, G. Ban, A. Battala, J. C. Vernhes, J. Tillier, N. Bellaize, C. Le Brun, B.
- 22 Tamain, K. Mercier and J. C. Motin, IEEE Trans. Nucl. Sci. **49 I** [5], 2223 (2002).
- 23 39) M. Ishikawa, N. Nagase, T. Matsuura, J. Hiratsuka, R. Suzuki, N. Miyamoto, K. L. Sutherland, K.
- 24 Fujita and H. Shirato, J. Radiat. Res. **56** [2], 372 (2015).
- 25 40) P. Carrasco, N. Jornet, O. Jordi, M. Lizondo, A. Latorre-Musoll, T. Eudaldo, A. Ruiz and M. Ribas,
- 26 Med. Phys. **42** [1], 297 (2015).

- 1 41) S. Takagi, T. Yaegashi and M. Ishikawa, Acad. Radiol. **26** [7], e174 (2019).
- 2 42) F. Alsanea, F. Therriault-Proulx, G. Sawakuchi and S. Beddar, Med. Phys. **45** [4], 1782 (2018).
- 3 43) C. Penner, C. Hoehr, S. O’Keeffe, P. Woulfe and C. Duzenli, IEEE Sens. J. **18** [4], 1513 (2018).
- 4 44) C. Hoehr, A. Morana, O. Duhamel, B. Capoen, M. Trinczek, P. Paillet, C. Duzenli, M. Bouazaoui, G.
5 Bouwmans, A. Cassez, Y. Ouerdane, A. Boukenter, H. El Hamzaoui and S. Girard, Sci. Rep. **9** [1], 4
6 (2019).
- 7 45) J. B. Birks, *The Theory and Practice of Scintillation Counting* (Elsevier, 1964).
- 8 46) M. Ishikawa, K. Ono, Y. Sakurai, H. Unesaki, A. Uritani, G. Bengua, T. Kobayashi, K. Tanaka and T.
9 Kosako, Appl. Radiat. Isot. **61** [5], 775 (2004).
- 10 47) M. Ishikawa, H. Kumada, K. Yamamoto, J. Kaneko, G. Bengua, H. Unesaki, Y. Sakurai, K. Tanaka
11 and T. Kosako, Nucl. Instruments Methods Phys. Res. Sect. A Accel. Spectrometers, Detect. Assoc.
12 Equip. **551** [2–3], 448 (2005).
- 13 48) M. Komeda, H. Kumada, M. Ishikawa, T. Nakamura, K. Yamamoto and A. Matsumura, Appl.
14 Radiat. Isot. **67** [7-8 SUPPL.], 254 (2009).
- 15 49) M. Ishikawa, T. Yamamoto, A. Matsumura, J. Hiratsuka, S. I. Miyatake, I. Kato, Y. Sakurai, H.
16 Kumada, S. J. Shrestha and K. Ono, Radiat. Oncol. **11** [1], 1 (2016).
- 17 50) Y. Ito, G. Katano, H. Harano, T. Matsumoto, A. Uritani, K. Kudo, K. Kobayashi, T. Yoshimoto, Y.
18 Sakurai, T. Kobayashi and C. Mori, Radiat. Prot. Dosimetry **110** [1–4], 619 (2004).
- 19 51) T. Matsumoto, H. Harano, A. Masuda, J. Nishiyama, Y. Sakurai and A. Uritani, Radiat. Prot.
20 Dosimetry **146** [1–3], 92 (2011).
- 21 52) K. Watanabe, Y. Kawabata, A. Yamazaki, A. Uritani, T. Iguchi, K. Fukuda and T. Yanagida, Nucl.
22 Instruments Methods Phys. Res. Sect. A Accel. Spectrometers, Detect. Assoc. Equip. **802**, 1 (2015).
- 23 53) A. Ishikawa, A. Yamazaki, K. Watanabe, S. Yoshihashi, A. Uritani, K. Fukuda, A. Koike, R.
24 Ogawara, M. Suda and T. Hamano, Nucl. Instruments Methods Phys. Res. Sect. A Accel.
25 Spectrometers, Detect. Assoc. Equip. **954** [August 2019], 161661 (2020).
- 26 54) A. Ishikawa, A. Yamazaki, K. Watanabe, S. Yoshihashi, A. Uritani, Y. Tsurita, K. Tsuchida and Y.

- 1 Kiyonagi, Radiat. Meas. [DOI:10.1016/j.radmeas.2020.106270].
- 2 55) K. Watanabe, S. Yoshihashi, A. Ishikawa, S. Honda, A. Yamazaki, Y. Tsurita, A. Uritani, K.
- 3 Tsuchida and Y. Kiyonagi, Appl. Radiat. Isot. [DOI:10.1016/j.apradiso.2020.109553].
- 4 56) A. Ishikawa, A. Yamazaki, K. Watanabe, S. Yoshihashi, A. Uritani, Y. Sakurai, H. Tanaka, R.
- 5 Ogawara, M. Suda and T. Hamano, Sensors Mater. **32** [4], 1489 (2020).
- 6 57) A. Ishikawa, K. Watanabe, A. Yamazaki, S. Yoshihashi, S. Imai, A. Masuda, T. Matsumoto, H.
- 7 Tanaka, Y. Sakurai, M. Nogami, K. Hitomi, A. Uritani and H. Harano, Nucl. Instruments Methods
- 8 Phys. Res. Sect. A Accel. Spectrometers, Detect. Assoc. Equip. [DOI:10.1016/j.nima.2021.166074].
- 9 58) K. Nagasawa, Y. Hoshi, Y. Ohki and K. Yahagi, Jpn. J. Appl. Phys. **24** [9R], 1224 (1985).
- 10 59) T. Kakuta, T. Shikama, M. Narui and T. Sagawa, Fusion Eng. Des. **41** [1–4], 201 (1998).
- 11 60) M. A. Eronyan, D. R. Devetyarov, A. A. Reytskii, I. K. Meshkovskiy, A. A. Untilov and A. A.
- 12 Pechenkin, Mater. Lett. **292**, 129628 (2021).
- 13 61) E. Takada, Y. Hosono, T. Kakuta, M. Yamazaki, H. Takahashi and M. Nakazawa, IEEE Trans. Nucl.
- 14 Sci. **45** [3], 556 (1998).
- 15 62) K. Toh, T. Nakamura, H. Yamagishi, K. Sakasai, K. Soyama and T. Shikama, Nucl. Instruments
- 16 Methods Phys. Res. Sect. A Accel. Spectrometers, Detect. Assoc. Equip. **700**, 130 (2013).
- 17 63) T. Yanagida and H. Sato, Opt. Mater. (Amst). **38**, 174 (2014).

Figure Captions

- Fig. 1** Schematic drawing of a) the Snell's law and b) the total internal reflection.
- Fig. 2** Geometrical relation on pathways of scintillation photons in the optical fiber. a) Light transmission mode in the optical fiber. b) Acceptable angle of scintillation photons into the optical fiber. c) Photons entering from a side surface of an optical fiber.
- Fig. 3** A fundamental configuration of the optical-fiber-based scintillation detector.
- Fig. 4** Schematic drawing of the wavelength-shifting fiber.
- Fig. 5** The concept of gamma-ray suppression by controlling the scintillator size.
- Fig. 6** Pulse height spectra obtained from the optical-fiber-based neutron detector using Eu:LiCaAlF₆ scintillator when irradiated with neutrons and gamma rays.

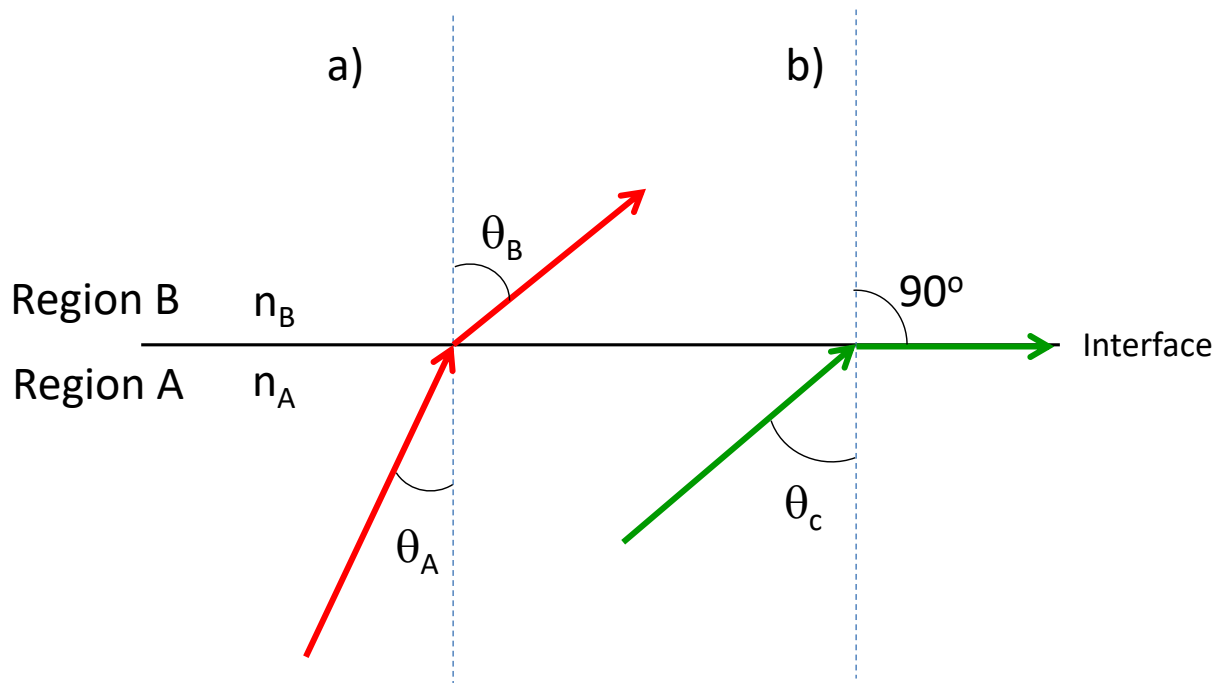


Fig. 1 Schematic drawing of a) the Snell's law and b) the total internal reflection.

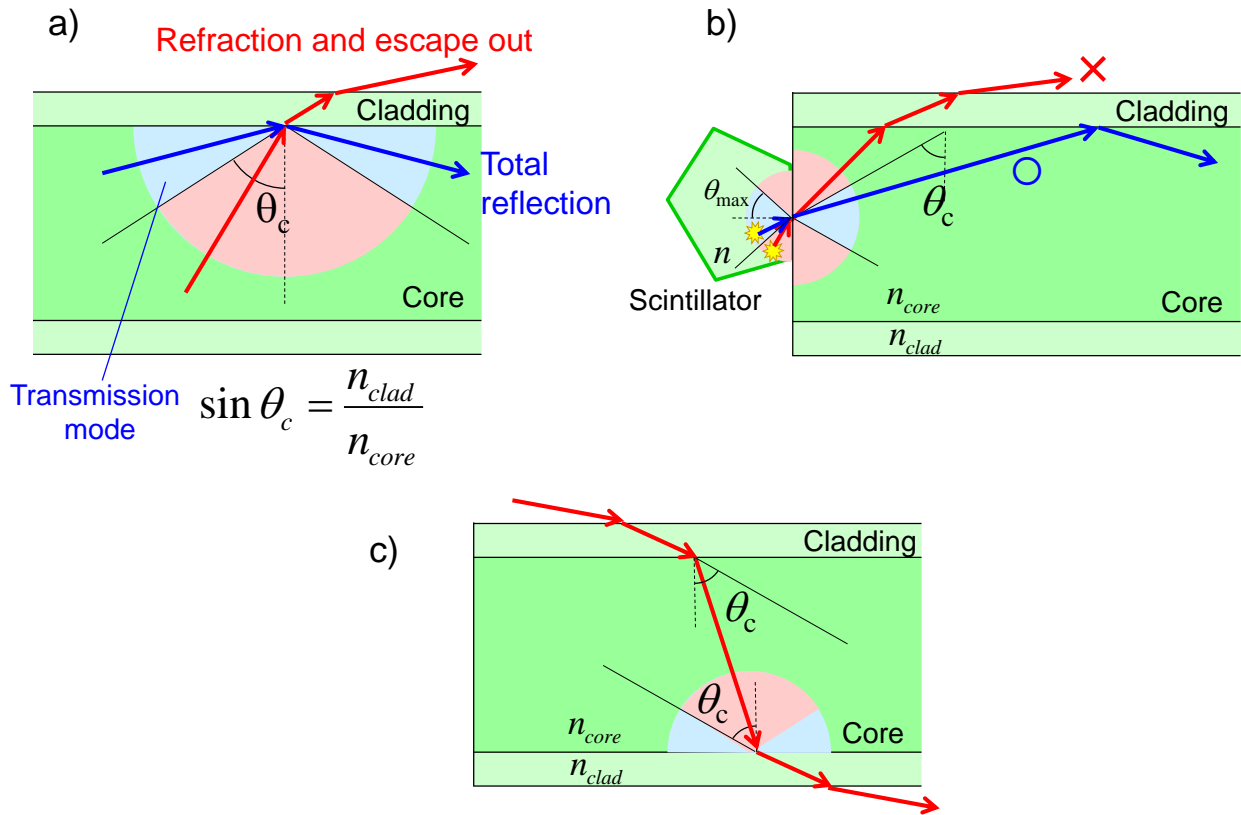


Fig. 2 Geometrical relation on pathways of scintillation photons in the optical fiber. a) Light transmission mode in the optical fiber. b) Acceptable angle of scintillation photons into the optical fiber. c) Photons entering from a side surface of an optical fiber.

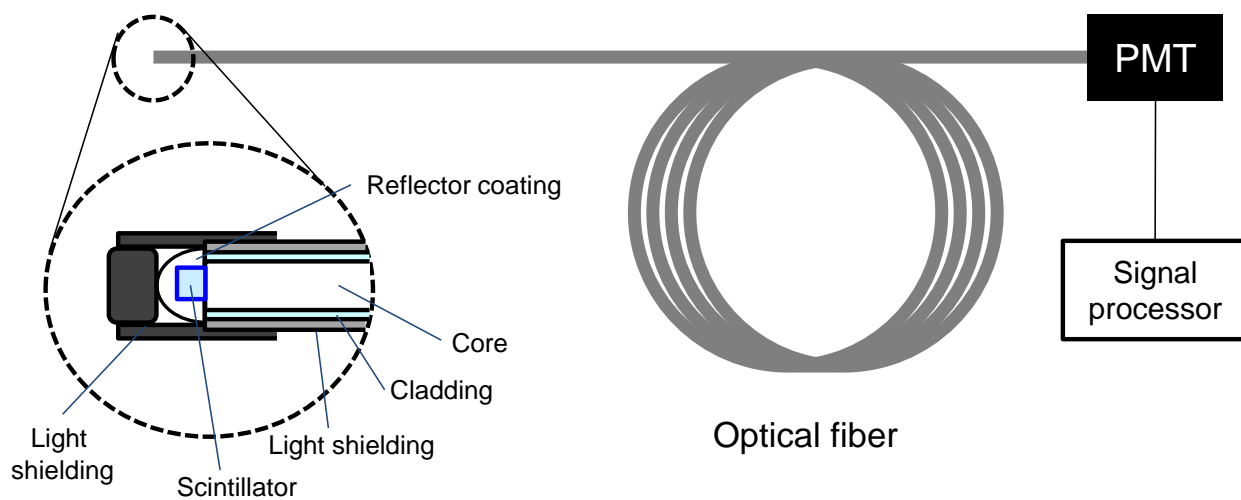


Fig. 3 A fundamental configuration of the optical-fiber-based scintillation detector.

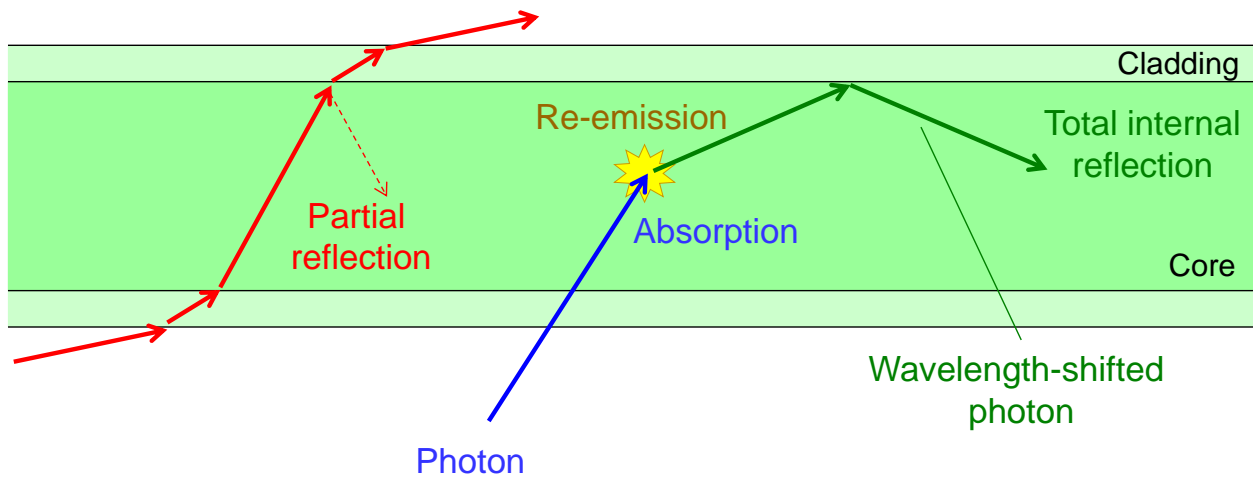
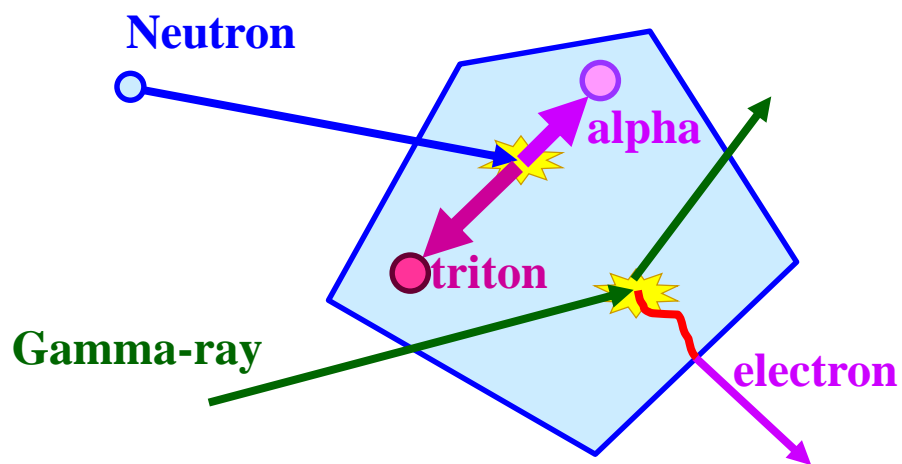


Fig. 4 Schematic drawing of the wavelength-shifting fiber.

1
2
3
4
5

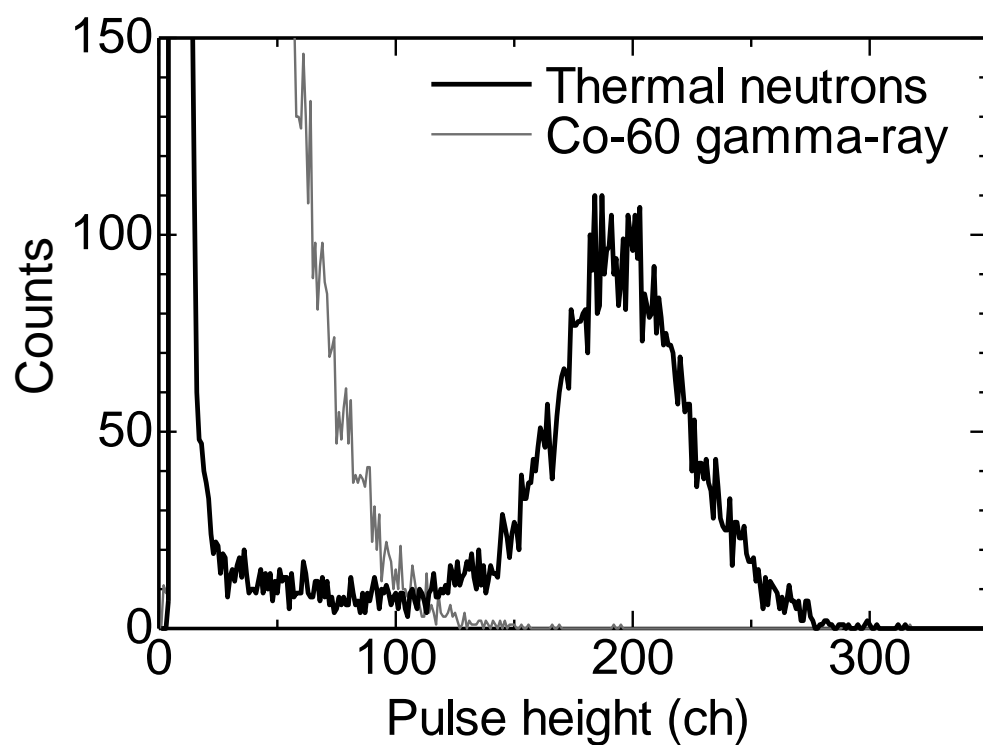


6
7
8
9
10
11

Fig. 5

The concept of gamma-ray suppression by controlling the scintillator size.

1
2
3



4
5
6
7
8
9

Fig. 6 Pulse height spectra obtained from the optical-fiber-based neutron detector using Eu:LiCaAlF₆ scintillator when irradiated with neutrons and gamma rays.